Title
Glioblastoma Induces Vascular Dysregulation in Nonenhancing Peritumoral Regions in Humans.

Journal
American Journal of Roentgenology, 206(5)

ISSN
0361-803X

Authors
Chow, Daniel S
Horenstein, Craig I
Canoll, Peter
et al.

Publication Date
2016-05-01

DOI
10.2214/ajr.15.14529

Peer reviewed

HHS Public Access

Author manuscript

AJR Am J Roentgenol. Author manuscript; available in PMC 2017 May 01.

Published in final edited form as:

AJR Am J Roentgenol. 2016 May ; 206(5): 1073–1081. doi:10.2214/AJR.15.14529.

Glioblastoma Induces Vascular Dysregulation in Nonenhancing Peritumoral Regions in Humans

Daniel S. Chow[1,2], **Craig I. Horenstein**[3], **Peter Canoll**[4], **Angela Lignelli**[1], **Elizabeth M. C. Hillman**[1,5], **Christopher G. Filippi**[1,3], and **Jack Grinband**[1]

[1]Department of Radiology, College of Physicians and Surgeons, Columbia University, New York, NY

[2]Department of Radiology and Biomedical Imaging, University of California, San Francisco, 505 Parnassus Ave, L352, San Francisco, CA 94143-0628

[3]Department of Radiology, North Shore University Hospital, Long Island, NY

[4]Department of Pathology and Cell Biology, College of Physicians and Surgeons, Columbia University, New York, NY

[5]Department of Biomedical Engineering, Columbia University, New York, NY

Abstract

OBJECTIVE—Glioblastoma is an invasive primary brain malignancy that typically infiltrates the surrounding tissue with malignant cells. It disrupts cerebral blood flow through a variety of biomechanical and biochemical mechanisms. Thus, neuroimaging focused on identifying regions of vascular dysregulation may reveal a marker of tumor spread. The purpose of this study was to use blood oxygenation level–dependent (BOLD) functional MRI (fMRI) to compare the temporal dynamics of the enhancing portion of a tumor with those of brain regions without apparent tumors.

MATERIALS AND METHODS—Patients with pathologically proven glioblastoma underwent preoperative resting-state BOLD fMRI, T1-weighted contrast-enhanced MRI, and FLAIR MRI. The contralesional control hemisphere, contrast-enhancing tumor, and peritumoral edema were segmented by use of structural images and were used to extract the time series of these respective regions. The parameter estimates (beta values) for the two regressors and resulting *z*-statistic images were used as a metric to compare the similarity of the tumor dynamics to those of other brain regions.

RESULTS—The time course of the contrast-enhancing tumor was significantly different from that of the rest of the brain ($p < 0.05$). Similarly, the control signal intensity was significantly different from the tumor signal intensity ($p < 0.05$). Notably, the temporal dynamics in the peritumoral edema, which did not contain enhancing tumor, were most similar to the those of enhancing tumor than to those of control regions.

Address correspondence to D. S. Chow (daniel.chow@ucsf.edu; jg2269@columbia.edu).

CONCLUSION—The findings show that the disruption in vascular regulation induced by a glioblastoma can be detected with BOLD fMRI and that the spatial distribution of these disruptions is localized to the immediate vicinity of the tumor and peritumoral edema.

Keywords

functional imaging; glioblastoma; neurovascular coupling; resting-state functional MRI; vascular dysregulation

Glioblastoma is a highly vascularized angiogenic tumor that induces a variety of abnormalities that cause vascular dysregulation [1]. Results with rodent models have shown that during abluminal cell migration, glioma cells surround existing blood vessels and displace the astrocytic end-feet covering the vascular surface. This disrupts astrocytic control of vascular tone in arteriolar smooth muscle [2]. Furthermore, displacement of astrocytes leads to destabilization of the basement membrane and down-regulation of endothelial tight junctions [3–6], which result in a breach of the blood-brain barrier (BBB) [7]. Thus, results with rodent models suggest that disruption of astrocytic control of vascular tone by end-foot displacement is strongly associated with breaches of the BBB. Though this phenomenon has been studied extensively in rodents, it is not known whether similar mechanisms operate in humans [1].

Problems of vascular regulation in and around tumors that have breached the BBB have been well documented in humans. For example, hypocapnic and hypercapnic challenges that normally cause vasoconstriction and dilation have reduced or no response around glioblastoma [8]. Within the contrast-enhancing region, perfusion-weighted imaging has shown elevated cerebral blood volume [9, 10]. PET [11], dynamic perfusion CT [12], and arterial spin labeling [13, 14] have all shown increases in cerebral blood flow. In addition, contrast-enhancing tumor regions also exhibit greater permeability on dynamic contrast-enhanced images [15], and the degree of permeability has been found to correlate with tumor grade [16]. In contrast, the region surrounding the contrast enhancement, identified as hyperintense FLAIR signal intensity, exhibits few abnormalities in cerebral blood flow, cerebral blood volume, or permeability [12, 13, 15, 17, 18]. Together, the results of these studies are consistent with those in rodent models of end-foot displacement: vascular regulation is impaired in contrast-enhancing (BBB breached) regions and appears normal in nonenhancing (BBB intact) regions.

Results of several studies, however, suggest possible vascular dysregulation in peritumoral nonenhancing regions. For example, direct optical imaging of the cortex has shown abnormal 0.1-Hz oscillations near an oligodendroglioma [19], and task-based blood oxygenation level–dependent (BOLD) functional MRI (fMRI) studies [20] have shown reductions in evoked activation near the tumor [21–23]. Although the finding was suggestive, the oligodendroglioma was part of a single case study, and task-based BOLD fMRI can have alternative explanations for reduced vascular responses, specifically that reductions may be due to neural rather than vascular deficits. Moreover, to test the hypothesis that vascular dysregulation and breaches of the BBB in humans are caused by the same mechanism in humans as in rodents, it is necessary to compare vascular function in the

contrast-enhancing region with vascular function in the peritumoral region. If end-foot displacement by glioma cells leads to both, then contrast-enhancing regions should exhibit vascular dysfunction, whereas nonenhancing regions should have normal vascular function. However, if the contrast-enhancing and noncontrast enhancing regions both show similar vascular dysregulation, then the mechanisms that disrupt vascular control and the BBB may be different from those proposed in rodents.

The purpose of this study was to characterize the variation in the BOLD signal intensity induced by the tumor to determine whether vascular dysregulation coincides with a breakdown in the BBB, as suggested by results of the aforementioned animal models of glioma infiltration. Specifically, we used resting-state fMRI to measure BOLD dynamics in patients with glioblastoma to determine whether impairments in vascular regulation are limited to regions with a breach of the BBB defined by areas of contrast enhancement; can be detected in abnormal, FLAIR hyperintense peritumoral brain regions; or are subject to both conditions. We also examined whether the tumor BOLD signal intensity detected in the peritumoral region varies as a function of distance from the tumor and whether the peritumoral region has an abnormal temporal profile relative to other brain regions.

Materials and Methods

Patient Selection

After institutional review board approval of this HIPAA-complaint study, a query of the neuropathology department at Columbia University Medical Center from January 2012 to November 2013 was conducted. Specifically, the records of patients who had undergone primary resection of glioblastoma and preoperative resting state fMRI were evaluated. A retrospective review of these medical records was conducted to determine demographic information, including sex and age. Patients with newly detected brain tumors who did not have a history of brain surgery or chemoradiation and who had undergone structural and functional imaging at Columbia University Medical Center for routine presurgical planning were included. Patients with recurrence or nonnative disease or with multifocal lesions were excluded.

Analysis Overview

The tumor, peritumoral, and control ROIs were identified on the structural images. The functional and structural images were then coregistered, and the BOLD signal intensity from the ROIs was extracted. Linear regression was performed to identify which voxels in the brain were correlated with the mean time series in the contrast-enhancing tumor and which were correlated with the mean time series of the control mask (Fig. 1A).

Image Acquisition

All imaging was performed with a 3-T MRI system (Signa, GE Healthcare) and an eight-channel head-array coil (Signa HDxt, GE Healthcare). Functional imaging was performed with the echoplanar imaging BOLD sequence (TR/TE, 2/34; FOV, 21 cm; matrix, 64 × 64; slice thickness, 5 mm; voxel size, 3.28 × 3.28 mm; acquisition duration, 6 minutes). We also performed FLAIR (TR/TE, 9000/156; inversion time, 2250 ms) and volumetric T1-weighted

unenhanced and contrast-enhanced sequences (T1-weighted 3D inversion recovery fast spoiled gradient-recalled sequence with the following parameters: TR/TE, 10.2/4.2 ms; inversion time, 450 ms; alpha, 13°; bandwidth, 25 kHz; FOV, 25 cm^2; matrix, 256 × 256; slice thickness, 1.2 mm). Contrast-enhanced images were acquired with IV gadobenate dimeglumine (MultiHance, Bracco) with a weight-based dose of 0.2 mL/kg. The time between IV injection and contrast-enhanced imaging was 5 minutes. BOLD images were obtained before contrast-enhanced imaging.

Tumor-Related ROIs

All tumor ROIs (Fig. 1B) were drawn by a neuroradiologist with a certificate of added qualification in neuroradiology and 17-years of experience. The ROI for the enhancing portion of the tumor was identified by calculating the difference of the unenhanced and contrast-enhanced T1-weighted images and manually drawing a mask around the enhancing portion. A separate mask was drawn around the necrotic center. The ROI of the peritumoral region was identified by manually drawing a mask around the abnormal hyperintense white matter on the FLAIR image. Then the enhancing tumor mask and the necrotic center mask were subtracted from the peritumoral mask to generate the final mask of the peritumoral region. Three sets of control masks were created in the contralesional hemisphere: the entire contralesional hemisphere, the contralesional white matter, and the contralesional gray matter. Gray and white matter segmentation for the contralesional masks was performed with the Centre for Functional MRI of the Brain (FMRIB) automated segmentation tool [24].

All ROIs were defined on the high-resolution structural images (1 mm × 1 mm × 1.2 mm). To generate the functional ROIs, which were collected at lower spatial resolution (3.28 mm × 3.28 mm × 5 mm), functional images were registered to structural images (6 *df*, linear), and the transformation matrix was applied to the ROIs to put them into functional space. To minimize any influence from nonenhancing portions of the surrounding tissue due to partial volume effects, the masks were thresholded such that the partial volume fraction of enhancing tumor was at least 0.95. No spatial smoothing was applied to the functional data to ensure that the BOLD signals from adjacent regions were not averaged together.

Image Processing

All data were processed with FMRIB Software Library (FSL version 5.0.6) [25] and Matlab (2012b, MathWorks) software. Tissue segmentation was performed with the FMRIB automated segmentation tool, and linear registration was applied with the FMRIB linear registration tool. Each functional image was motion corrected, slice timing corrected, and skull stripped. No spatial or temporal filtering was performed before the regression analyses to minimize the mixing of signal intensity from adjacent brain regions. To minimize the effect of head motion on BOLD signal intensity, the motion parameters were regressed out of the data before regression was performed with the tumor and control time series. The 18 motion regressors used in the regression model consisted of three translations, three rotations, the first derivative of each, and the square of each. We also included a CSF regressor, extracted from the ventricles, to represent nonvascular artifacts. The final regression model consisted of 20 regressors (18 motion, one CSF regressor, and the

intercept) and was run during preprocessing. The residual from this model was then used for all subsequent regression analyses of tumor and control ROIs.

Blood Oxygenation Level–Dependent MRI Dynamics

We extracted the BOLD time series from the ROI defined by the contrast-enhancing portion of the tumor (Fig. 1C). We extracted the BOLD time series for the contralesional control hemisphere by averaging all voxels within the control mask. The BOLD signal intensity for the contralesional hemisphere is similar to the global mean signal intensity, which is often included in the regression model in studies of functional connectivity as a means of controlling for BOLD correlations that may stem from cardiac pulsations and respiration-related changes in arterial CO_2 [26–28]. However, it has also been found that the global signal intensity can reflect whole-brain fluctuations of neural origin [29]. Though this signal intensity is often considered a nuisance variable that is regressed out as part of the preprocessing of BOLD data [30, 31], in the current study the contralesional hemisphere signal intensity was used as a temporal signature of hemodynamics that reflects a normal response to cardiac pulsatility and respiration-related CO_2 changes or normal neural sources that are common across the whole brain. Multiple linear regression was performed according to the two-regressor model (Fig. 1C), that is, the enhancing tumor and contralesional control mean time series and their first derivatives to allow variation in timing. The output of this analysis and the metrics used to draw our conclusions consisted of parameter estimates (beta weights) and *z*-statistic values (beta weights normalized by the residual variance) for each voxel. All statistical analyses were performed with FSL and Matlab software with $p = 0.05$ and cluster corrected at $p = 0.05$ according to gaussian random field theory.

Blood Oxygenation Level–Dependent Signal Intensity Versus Distance

To assess the effect of distance on BOLD signal intensity, we tested whether the BOLD signal intensity in the peritumoral region changed as a function of distance from the contrast-enhancing region. For this analysis, the distance between each voxel in the peritumoral regions and the nearest contrast-enhancing voxel was calculated. The BOLD signal intensity for tumor and the BOLD signal intensity for control regions were then plotted as a function of nearest distance from the tumor. A regression analysis was performed for each patient to measure the effect of distance on the tumor signal intensity and on the control signal intensity. The parameter estimates of the slope were averaged across patients.

Proportion of Gray to White Matter

To measure the effect of proportion of gray to white matter in the control mask on estimates of vascular dysregulation, we extracted the *z*-statistics for each voxel in the peritumoral mask generated by the gray matter segmented control mask and by the white matter segmented control mask. The correlation was computed between the *z*-statistic values generated by the two control masks within the peritumoral region for each subject. The mean correlation across subjects was computed after performance of the Fisher *z* transform and applying the inverse of the Fisher *z* transform to the mean and SD.

Contrast Between Tumor and Control Regions

To determine whether combining the tumor and control maps results in improved contrast between the tumor and control voxels, we tested image contrast using the D prime statistic, as follows:

$$\frac{\text{mean } (z_{\text{tumor}}) - \text{mean } (z_{\text{control}})}{\sqrt{0.5(\sigma_{\text{tumor}}{}^2 + \sigma_{\text{control}}{}^2)}},$$

where z_{tumor} represents the z-statistic intensities from the voxels located within the contrast-enhancing tumor mask and σ_{tumor} represents the SD of those voxels. The D prime between the tumor and control regions was computed for each patient, and the mean D prime was plotted.

Results

Patient Selection

In total, we identified 14 patients (10 [71.4%] men, four [28.6%] women; mean age, 54.1 ± 11.2 [SD] years; range, 37–76 years) at the institution during the study period who had native disease and underwent BOLD resting-state fMRI before tumor resection. Patients with recurrent disease and previous treatment with chemotherapy or radiation therapy were excluded from the study.

Temporal Signature of Tumor and Contralesional Hemisphere

We tested whether the temporal dynamics of voxels within the tumor, as defined by the time series extracted from the contrast-enhancing tumor ROI, could be detected outside the contrast-enhancing boundary. Similarly, we tested whether the temporal dynamics of the control hemisphere were detectable inside the peritumoral and contrast-enhancing tumor boundaries. Figure 2 shows the z-statistic maps for the tumor and control regressors. As expected, the voxels inside the contrast-enhancing region show the strongest correlation with the tumor mean time series (Fig. 2, column 3). However, the nonenhancing peritumoral region also positively correlated with the tumor, and areas outside the peritumoral region were either very weakly correlated or not correlated with the tumor. In contrast, the contralesional hemisphere signal intensity exhibited strong correlations in areas outside the peritumoral region (Fig. 2, column 4) and was not correlated or was negatively correlated with the tumor. The peritumoral region exhibited intermediate correlation with the control signal intensity. Calculating the mean of all voxels within an ROI and averaging across the group (Fig. 3) showed significant differences between tumor and the peritumoral region and between peritumoral and control regions. The mean z-statistic for the tumor regressor was 3.15 (standard error [SE], 0.43) for the contrast-enhancing, 1.63 (SE, 0.22) for the peritumoral, and 0.13 (SE, 0.04) for the control regions. For the control regressor, the z-statistics were −0.001 (SE, 0.04), 0.78 (SE, 0.12), and 2.29 (SE, 0.20). The z-statistic differences between tumor and control were 1.78 (SE, 0.23), 0.45 (SE, 0.13), and −1.34 (SE, 0.15). We repeated this analysis using gray and white matter segmented control masks. The z-statistic maps in the peritumoral region generated with the gray matter and white matter

control masks showed mean correlation of 0.96 across the group. This suggests that the proportion of gray to white matter does not have a meaningful difference in estimates of vascular dysregulation.

Results of previous studies have suggested that glioblastoma infiltration is associated with a cell-density gradient whereby tumor cellularity is highest nearest the contrast enhancement and decreases with distance [32, 33]. To test whether such a gradient is detectable within the peritumoral region, we assessed the relation between the BOLD signal intensity for tumor and control and the distance to the nearest enhancing voxel. Figure 4A shows the distance relation for a single patient. The tumor signal intensity decreases as a function of distance, whereas the control signal intensity increases as a function of distance. All patients had a decrease in tumor signal intensity as a function of distance, and all but one had an increase in control signal intensity as a function of distance (Fig. 4B). The group mean was significant for both tumor and control signal intensity (Fig. 4C).

Temporal Dynamics of Tumor and Contralesional Hemisphere

Finally, we used spectral analysis to test whether the BOLD dynamics were abnormal in the tumor and peritumoral regions relative to control regions. The power spectrum (Fig. 5) did not show significant differences (t test, $p < 0.05$) when averaged across all voxels in each mask. A comparison of the time series from the tumor and control regions showed that only 11% of the variance was shared (Pearson $r = 0.33$; SE, 0.08). These data indicate similar spectral characteristics but a lack of correlation between tumor and control regions. Moreover, the lack of correlation suggests that combining the tumor and control measures may produce better tissue separation than either one alone. Subtraction of the control z-statistic map from the tumor z-statistic map (Fig. 6) shows regions with no apparent tumor as negative (blue) voxels and regions with contrast enhancement and abnormal FLAIR hyperintensity as positive (red) voxels. The z-statistic differences between tumor and control maps were as follows: mean enhancing tumor, 3.1 (SE, 0.45); mean peritumoral, 0.85 (SE, 0.19); mean control, −2.5 (SE, 0.22). Furthermore, the difference image had higher contrast (D prime, 1.52; SE, 0.50) than the control-only image (D prime, 1.17; SE, 0.24) and higher contrast than the tumor-only image (D prime, 1.36; SE, 0.62).

An interesting finding in some cases was that the BOLD signal intensity had a sharp boundary that did not match the FLAIR hyperintensity boundary. For example, the BOLD signal intensity boundary may have been within the FLAIR boundary (Fig. 6A, top middle) or outside the FLAIR boundary (Fig. 6A, top right or bottom middle). Though these results are speculative and ultimately require pathologic verification, they nevertheless suggest that BOLD dynamics may be useful for classifying the peritumoral region into normal and abnormal brain matter.

Discussion

It is well known that glioblastoma causes vascular dysregulation in contrast-enhancing regions. The dysregulation is characterized by reduced response to capneic challenges [34], elevated perfusion [9–12, 14, 17], and increased permeability [15, 16, 35–38]. However, the effect of nonenhancing infiltrating tumor on its local environment is poorly understood. In

this study, we used resting-state BOLD data in brain tumor patients and applied correlation analysis to discern a new peritumoral contrast we hypothesize to be the result of vascular disruption by infiltrating glioma cells. Previous work has shown that tumor cells can be found outside the contrast-enhancing region with density decreasing with distance [32, 33] and that extent of resection correlates with clinical outcome [39]. Though the results of those studies indicated that the leading edge of infiltration is beyond the contrast-enhancing region, it was not known whether nonenhancing tumor induces functional deficits. Our results show that the nonenhancing peritumoral region has BOLD dynamics similar to those of the contrast-enhancing regions of the tumor, indicating that tumor-induced vascular dysregulation does not require a breach in the BBB. This result further suggests that any disruptions in astrocyte-vascular interactions caused by end-foot displacement by glioma cells [5] are not necessarily associated with degradation of the basement membrane or down-regulation of tight junctions. Our data may represent a step in the infiltrative process that precedes vascular cooption by glioma cells. However, it is also possible that, in humans, direct parenchymal spread [40] of glioma cells allows the maintenance of an intact BBB while causing abnormalities in the microenvironment [41] of astrocytes that disrupt normal astrocyte-vascular interactions [2, 42].

Though previous work has shown that glioma cells can control vascular tone [5], it is unlikely that this mechanism can explain the similarity in BOLD activity between the enhancing tumor and peritumoral region. Glioblastoma tumors do not have any known means of rapidly signaling and coordinating biochemical actions across large regions of brain tissue, and thus, coherent fluctuations in vascular tone within the peritumoral region cannot be due to direct glioma-mediated vascular control. Because the BOLD signal originates primarily from capillary and venous changes in oxygenation levels, an alternative explanation of the similarity in tumoral and peritumoral BOLD activity may be common venous drainage between the two brain regions; that is, normal BOLD activity in the peritumoral regions may be masked by abnormal activity in the tumor as the blood from the two regions mixes together. Though this may be possible for very small tumors and peritumoral regions, it is unlikely for larger tumors and peritumoral regions that span many centimeters and have disparate drainage systems. We found that similarity between the two regions cannot be explained by distance effects (Fig. 3), suggesting distinct venous drainage in the tumor and peritumoral regions.

A more likely explanation for common activity is that glioma-induced disruption in vascular control reduces the influence of the neurovascular unit while revealing normally hidden, intrinsic fluctuations in vascular tone. Cerebral arteriolar diameter is modulated by both pressure [43, 44] and intraluminal flow [45–47], and in the absence of astrocytic end-feet, these intrinsic fluctuations may become visible, leading to apparent vascular compartmentalization (Figs. 1 and 5).

Previous fMRI studies have shown glioma-related reductions in BOLD activation [22, 23, 48]. Though these reductions can be caused by altered neuronal function due to tumor-induced toxicity, our data suggest they may also be related to disruptions in neurovascular coupling. Tumor-induced neurovascular uncoupling has been found with breath-holding during BOLD fMRI [49] and optical imaging [19].

Finally, we speculate that resting-state correlations may provide a robust signal for improving tissue segmentation and classification. Figure 5 shows that combining the *z*-statistic maps for tumor and control time series results in opposite signs for regions with and without apparent tumor. Furthermore, in some cases the peritumoral region with FLAIR hyperintensity exhibits a mixture of voxels, some having the BOLD signature of contrast-enhancing tumor and others having the BOLD signature of normal brain. Thus, it may be possible to use resting-state fMRI to identify the infiltrating edge of the tumor and segment the FLAIR hyperintensity into nonenhancing tumor and nontumor edema. Moreover, presurgical planning is centered on removal of the contrast-enhancing tumor. Thus, future work must assess whether removal of regions characterized by vascular dysregulation affects clinical outcome. This study was retrospective, and no biopsy results were available. Therefore, histopathologic studies are needed to determine the degree of infiltration that can produce detectable vascular dysregulation and to verify that combining the tumor and control signal intensities into a single measure improves tissue classification.

Acknowledgments

Supported by Radiological Society of North America grant RR1312 (D. S. Chow); National Institutes of Health (NIH) grant R01NS066955-01 (P. Canoll); and NIH grants R01 NS076628 (National Institute of Neurological Disorders and Stroke [NINDS]) and NS063226 (NINDS), Clinical and Translational Science Award grant UL1 TR000040, and National Science Foundation grant 0954796 (E. M. C. Hillman).

References

1. Cuddapah VA, Robel S, Watkins S, Sontheimer H. A neurocentric perspective on glioma invasion. Nat Rev Neurosci. 2014; 15:455–465. [PubMed: 24946761]
2. Attwell D, Buchan AM, Charpak S, Lauritzen M, Macvicar BA, Newman EA. Glial and neuronal control of brain blood flow. Nature. 2010; 468:232–243. [PubMed: 21068832]
3. Holash J, Maisonpierre PC, Compton D, et al. Vessel cooption, regression, and growth in tumors mediated by angiopoietins and VEGF. Science. 1999; 284:1994–1998. [PubMed: 10373119]
4. Farin A, Suzuki SO, Weiker M, Goldman JE, Bruce JN, Canoll P. Transplanted glioma cells migrate and proliferate on host brain vasculature: a dynamic analysis. Glia. 2006; 53:799–808. [PubMed: 16541395]
5. Watkins S, Robel S, Kimbrough IF, Robert SM, Ellis-Davies G, Sontheimer H. Disruption of astrocyte-vascular coupling and the blood-brain barrier by invading glioma cells. Nat Commun. 2014; 5:4196. [PubMed: 24943270]
6. Zagzag D, Amirnovin R, Greco MA, et al. Vascular apoptosis and involution in gliomas precede neovascularization: a novel concept for glioma growth and angiogenesis. Lab Invest. 2000; 80:837–849. [PubMed: 10879735]
7. Persidsky Y, Ramirez SH, Haorah J, Kanmogne GD. Blood-brain barrier: structural components and function under physiologic and pathologic conditions. J Neuroimmune Pharmacol. 2006; 1:223–236. [PubMed: 18040800]
8. Pronin IN, Holodny AI, Kornienko VN, Petraikin AV, Golovanov AV, Lee HJ. The use of hyperventilation in contrast-enhanced MR of brain tumors. AJNR. 1997; 18:1705–1708. [PubMed: 9367318]
9. Calli C, Kitis O, Yunten N, Yurtseven T, Islekel S, Akalin T. Perfusion and diffusion MR imaging in enhancing malignant cerebral tumors. Eur J Radiol. 2006; 58:394–403. [PubMed: 16527438]
10. Hakyemez B, Erdogan C, Bolca N, Yildirim N, Gokalp G, Parlak M. Evaluation of different cerebral mass lesions by perfusion-weighted MR imaging. J Magn Reson Imaging. 2006; 24:817–824. [PubMed: 16958061]

11. Tyler JL, Diksic M, Villemure JG, et al. Metabolic and hemodynamic evaluation of gliomas using positron emission tomography. J Nucl Med. 1987; 28:1123–1133. [PubMed: 3496433]
12. Schramm P, Xyda A, Klotz E, Tronnier V, Knauth M, Hartmann M. Dynamic CT perfusion imaging of intra-axial brain tumours: differentiation of high-grade gliomas from primary CNS lymphomas. Eur Radiol. 2010; 20:2482–2490. [PubMed: 20495977]
13. Noguchi T, Yoshiura T, Hiwatashi A, et al. Perfusion imaging of brain tumors using arterial spin-labeling: correlation with histopathologic vascular density. AJNR. 2008; 29:688–693. [PubMed: 18184842]
14. Tourdias T, Rodrigo S, Oppenheim C, et al. Pulsed arterial spin labeling applications in brain tumors: practical review. J Neuroradiol. 2008; 35:79–89. [PubMed: 18206239]
15. Cha S, Yang L, Johnson G, et al. Comparison of microvascular permeability measurements, K(trans), determined with conventional steady-state T1-weighted and first-pass T2*-weighted MR imaging methods in gliomas and meningiomas. AJNR. 2006; 27:409–417. [PubMed: 16484420]
16. Roberts HC, Roberts TP, Brasch RC, Dillon WP. Quantitative measurement of microvascular permeability in human brain tumors achieved using dynamic contrast-enhanced MR imaging: correlation with histologic grade. AJNR. 2000; 21:891–899. [PubMed: 10815665]
17. Chawla S, Wang S, Wolf RL, et al. Arterial spin-labeling and MR spectroscopy in the differentiation of gliomas. AJNR. 2007; 28:1683–1689. [PubMed: 17893221]
18. Kim HS, Kim SY. A prospective study on the added value of pulsed arterial spin-labeling and apparent diffusion coefficients in the grading of gliomas. AJNR. 2007; 28:1693–1699. [PubMed: 17885229]
19. Rayshubskiy A, Wojtasiewicz TJ, Mikell CB, et al. Direct, intraoperative observation of ~0.1 Hz hemodynamic oscillations in awake human cortex: implications for fMRI. Neuroimage. 2014; 87:323–331. [PubMed: 24185013]
20. Lee MH, Smyser CD, Shimony JS. Resting-state fMRI: a review of methods and clinical applications. AJNR. 2013; 34:1866–1872. [PubMed: 22936095]
21. Schreiber A, Hubbe U, Ziyeh S, Hennig J. The influence of gliomas and nonglial space-occupying lesions on blood-oxygen-level-dependent contrast enhancement. AJNR. 2000; 21:1055–1063. [PubMed: 10871013]
22. Jiang Z, Krainik A, David O, et al. Impaired fMRI activation in patients with primary brain tumors. Neuroimage. 2010; 52:538–548. [PubMed: 20452442]
23. Holodny AI, Schulder M, Liu WC, Maldjian JA, Kalnin AJ. Decreased BOLD functional MR activation of the motor and sensory cortices adjacent to a glioblastoma multiforme: implications for image-guided neurosurgery. AJNR. 1999; 20:609–612. [PubMed: 10319970]
24. Zhang Y, Brady M, Smith S. Segmentation of brain MR images through a hidden Markov random field model and the expectation-maximization algorithm. IEEE Trans Med Imaging. 2001; 20:45–57. [PubMed: 11293691]
25. Jenkinson M, Beckmann CF, Behrens TE, Woolrich MW, Smith SM. FSL. Neuroimage. 2012; 62:782–790. [PubMed: 21979382]
26. Shmueli K, van Gelderen P, de Zwart JA, et al. Low-frequency fluctuations in the cardiac rate as a source of variance in the resting-state fMRI BOLD signal. Neuroimage. 2007; 38:306–320. [PubMed: 17869543]
27. Murphy K, Birn RM, Handwerker DA, Jones TB, Bandettini PA. The impact of global signal regression on resting state correlations: are anti-correlated networks introduced? Neuroimage. 2009; 44:893–905. [PubMed: 18976716]
28. Birn RM, Murphy K, Bandettini PA. The effect of respiration variations on independent component analysis results of resting state functional connectivity. Hum Brain Mapp. 2008; 29:740–750. [PubMed: 18438886]
29. Schölvinck ML, Maier A, Ye FQ, Duyn JH, Leopold DA. Neural basis of global resting-state fMRI activity. Proc Natl Acad Sci USA. 2010; 107:10238–10243. [PubMed: 20439733]
30. Murphy K, Birn RM, Bandettini PA. Resting-state fMRI confounds and cleanup. Neuroimage. 2013; 80:349–359. [PubMed: 23571418]
31. Desjardins AE, Kiehl KA, Liddle PF. Removal of confounding effects of global signal in functional MRI analyses. Neuroimage. 2001; 13:751–758. [PubMed: 11305902]

32. Kelly PJ. Computed tomography and histologic limits in glial neoplasms: tumor types and selection for volumetric resection. Surg Neurol. 1993; 39:458–465. [PubMed: 8390726]
33. Pallud J, Varlet P, Devaux B, et al. Diffuse low-grade oligodendrogliomas extend beyond MRI-defined abnormalities. Neurology. 2010; 74:1724–1731. [PubMed: 20498440]
34. Bradac GB, Simon RS, Heidsieck CH. Angiographically verified transient alteration of the intracranial arteries and veins in dependence of different CO2 tensions. Neuroradiology. 1976; 10:257–262. [PubMed: 945488]
35. Larsson HB, Tofts PS. Measurement of blood-brain barrier permeability using dynamic Gd-DTPA scanning—a comparison of methods. Magn Reson Med. 1992; 24:174–176. [PubMed: 1556924]
36. Schwickert HC, Stiskal M, Roberts TP, et al. Contrast-enhanced MR imaging assessment of tumor capillary permeability: effect of irradiation on delivery of chemotherapy. Radiology. 1996; 198:893–898. [PubMed: 8628889]
37. Bergamino M, Saitta L, Barletta L, et al. Measurement of blood-brain barrier permeability with t1-weighted dynamic contrast-enhanced MRI in brain tumors: a comparative study with two different algorithms. ISRN Neurosci. 2013; 2013:905279. [PubMed: 24959569]
38. Daldrup H, Shames DM, Wendland M, et al. Correlation of dynamic contrast-enhanced MR imaging with histologic tumor grade: comparison of macromolecular and small-molecular contrast media. AJR. 1998; 171:941–949. [PubMed: 9762973]
39. Hardesty DA, Sanai N. The value of glioma extent of resection in the modern neurosurgical era. Front Neurol. 2012; 3:140. [PubMed: 23087667]
40. Goldbrunner RH, Bernstein JJ, Tonn JC. Cell-extracellular matrix interaction in glioma invasion. Acta Neurochir. 1999; 141:295–305. discussion, 304–305. [PubMed: 10214487]
41. Xie Q, Mittal S, Berens ME. Targeting adaptive glioblastoma: an overview of proliferation and invasion. Neuro Oncol. 2014; 16:1575–1584. [PubMed: 25082799]
42. Hillman EM. Coupling mechanism and significance of the BOLD signal: a status report. Annu Rev Neurosci. 2014; 37:161–181. [PubMed: 25032494]
43. Golding EM, Robertson CS, Bryan RM Jr. Comparison of the myogenic response in rat cerebral arteries of different calibers. Brain Res. 1998; 785:293–298. [PubMed: 9518656]
44. Wallis SJ, Firth J, Dunn WR. Pressure-induced myogenic responses in human isolated cerebral resistance arteries. Stroke. 1996; 27:2287–2290. discussion, 2291. [PubMed: 8969795]
45. Madden JA, Christman NJ. Integrin signaling, free radicals, and tyrosine kinase mediate flow constriction in isolated cerebral arteries. Am J Physiol. 1999; 277:H2264–H2271. [PubMed: 10600845]
46. Ngai AC, Winn HR. Modulation of cerebral arteriolar diameter by intraluminal flow and pressure. Circ Res. 1995; 77:832–840. [PubMed: 7554130]
47. Shimoda LA, Norins NA, Jeutter DC, Madden JA. Flow-induced responses in piglet isolated cerebral arteries. Pediatr Res. 1996; 39:574–583. [PubMed: 8848328]
48. Hou BL, Bradbury M, Peck KK, Petrovich NM, Gutin PH, Holodny AI. Effect of brain tumor neovasculature defined by rCBV on BOLD fMRI activation volume in the primary motor cortex. Neuroimage. 2006; 32:489–497. [PubMed: 16806983]
49. Zaca D, Hua J, Pillai JJ. Cerebrovascular reactivity mapping for brain tumor presurgical planning. World J Clin Oncol. 2011; 2:289–298. [PubMed: 21773079]

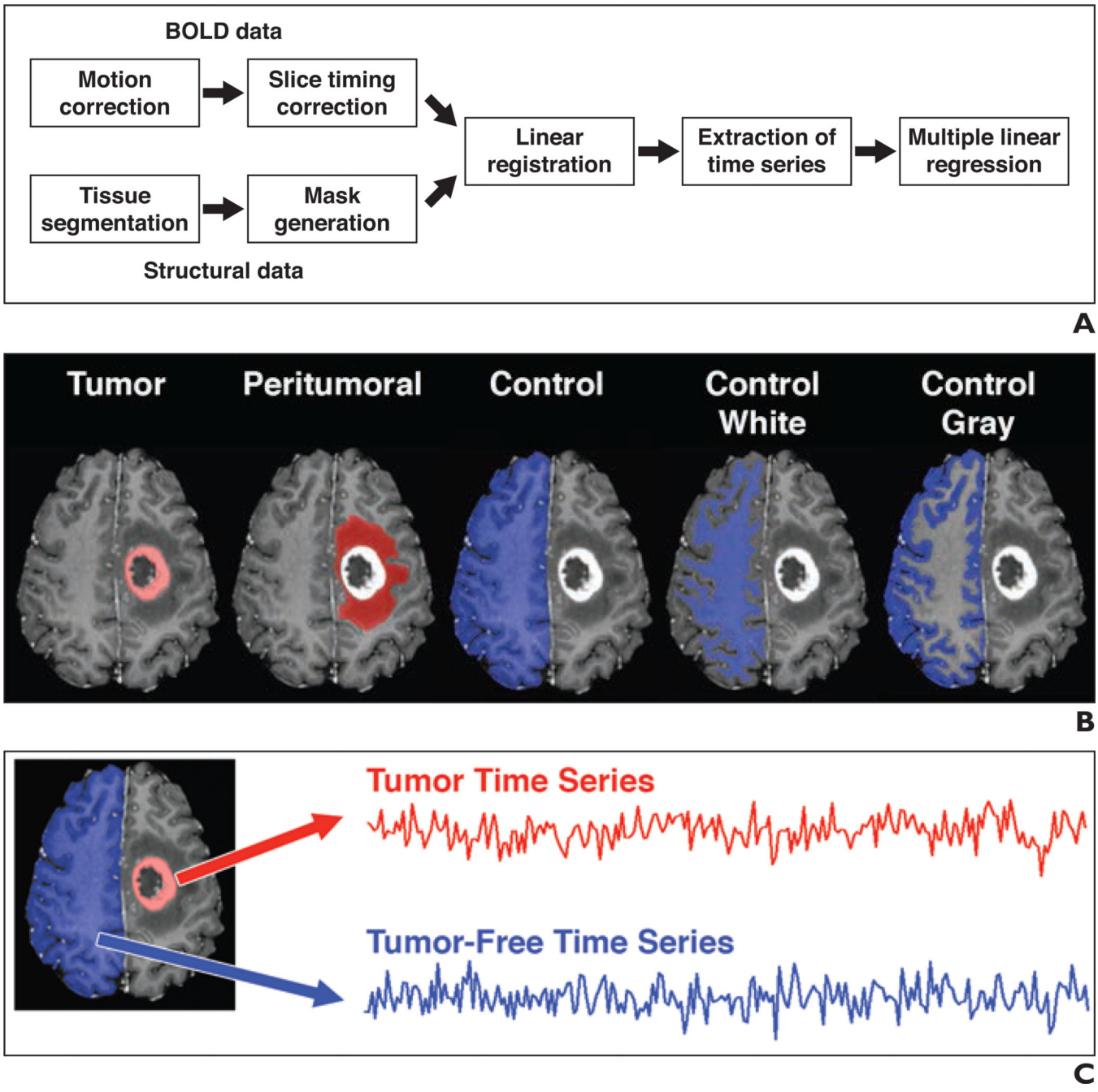

Fig. 1. Methods

A, Chart shows analysis pipeline consisting of tissue segmentation and mask creation from T1-weighted plus contrast-enhanced and FLAIR images. Blood oxygenation level–dependent (BOLD) data were motion- and slice-timing corrected and registered to structural images. Masks were transformed from structural to functional space, and time series were extracted from each mask. Multiple regression was performed with time series as regressors. **B,** MR images show volumetric masks of contrast-enhancing tumor and peritumoral FLAIR hyperintensity drawn by radiologist. Control masks consisted of contralesional hemisphere and contralesional white and gray matter segmentations.

C, MR image shows that for each patient, time series was extracted from control mask and contrast-enhancing tumor mask. Time series were assumed to represent normal (control mask) and tumor tissue (contrast-enhancing mask) and were used as regressors in linear regression model.

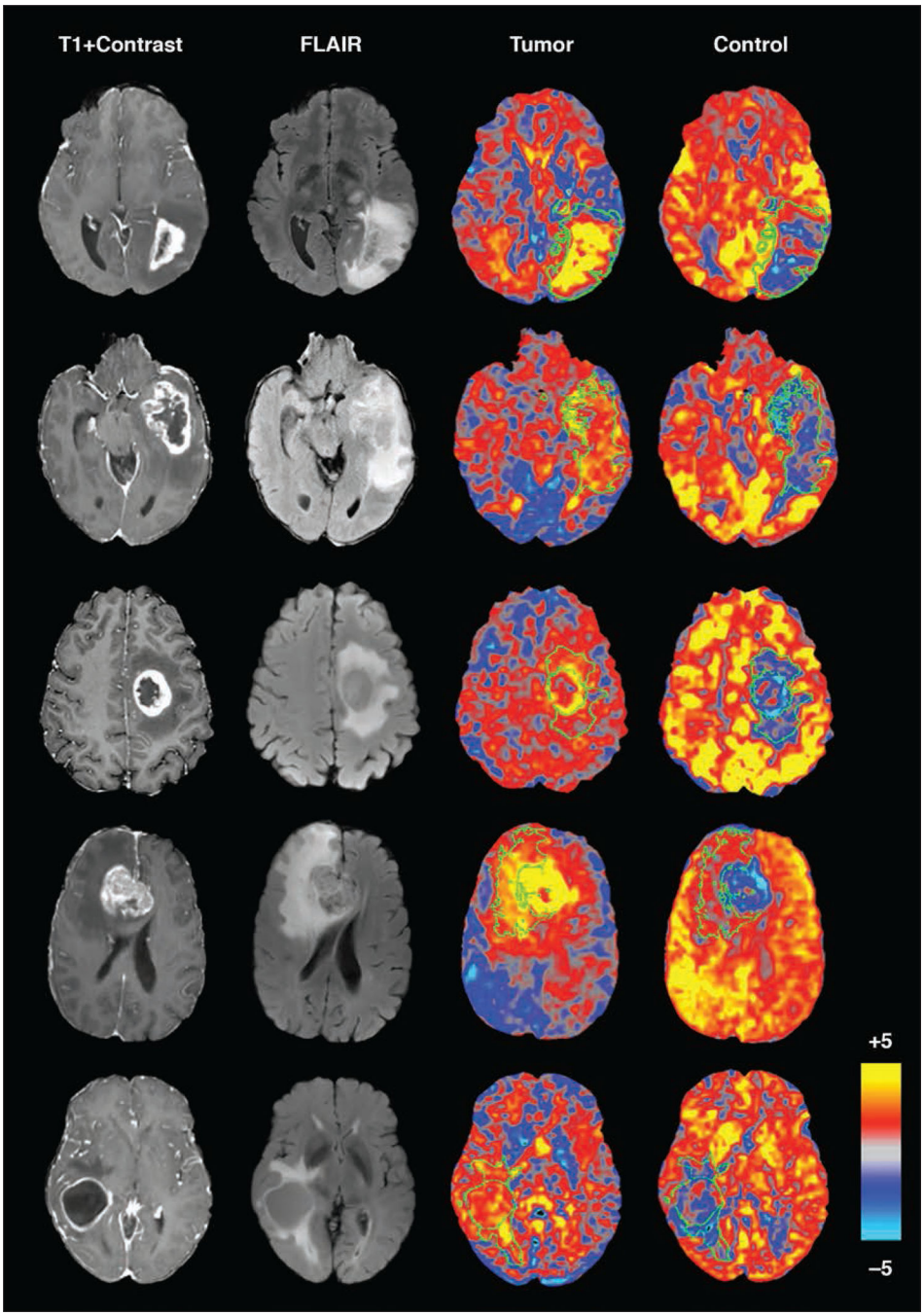

Fig. 2. ***Top to bottom*****, 35-year-old woman, 54-year-old man, 35-year-old man, 61-year-old man, and 57-year-old woman with glioblastoma**

Contrast-enhanced T1-weighted and FLAIR images show location of enhancing tumor and peritumoral regions. Columns 3 and 4 show *z*-statistic maps of enhancing tumor time series and control time series and represent strength of relation between regressors and each voxel. Outline of peritumoral region is overlaid on top of *z*-statistic maps. As expected, highest *z*-statistic values for tumor time series are inside enhancing portion of tumor. Peritumoral region also exhibits strong relation to enhancing tumor. Control time series is positively

correlated with most voxels outside enhancing tumor and has low or negative correlation in peritumoral region.

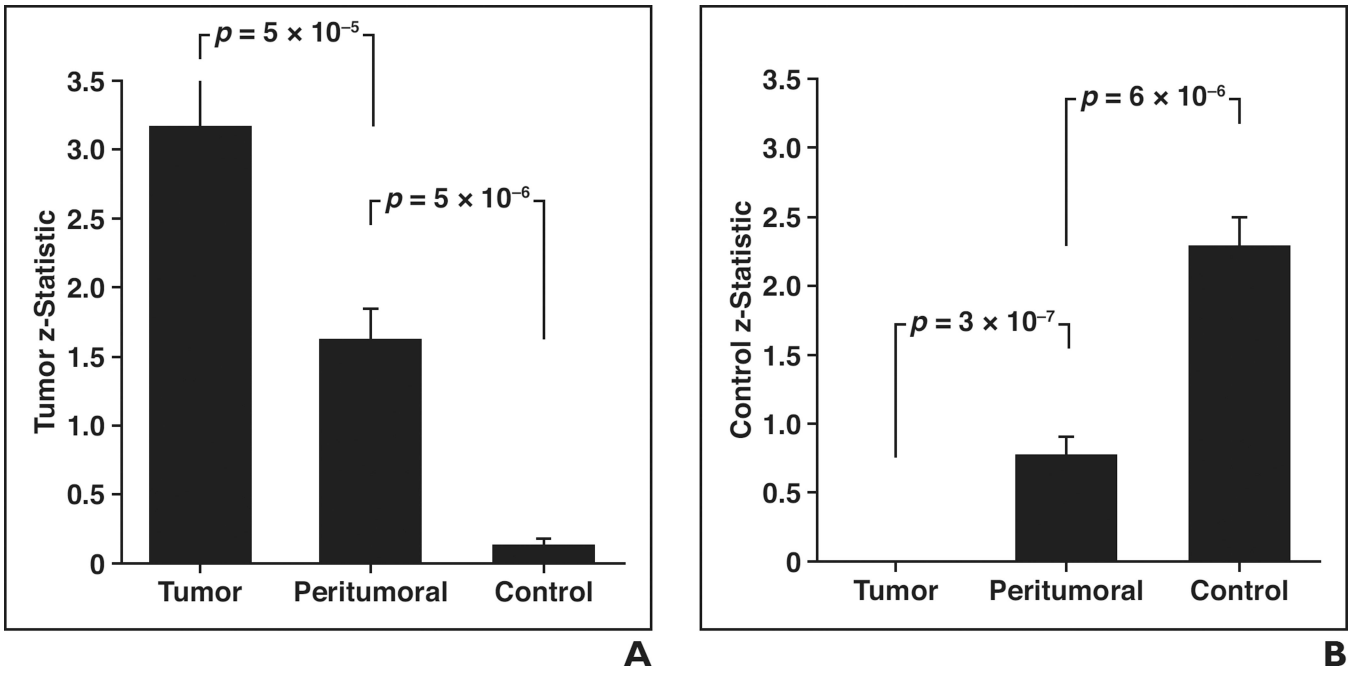

Fig. 3. Group means

Z-statistics for enhancing tumor time series averaged across subjects ($n = 14$). **A,** Graph shows mean time series of tumor region has highest correlation with voxels within tumor and fluctuates around zero in control regions. Peritumoral region has values midway between tumor and control. Error bars represent standard error, and all pairwise comparisons are significant. (Tumor regressor was constructed by averaging time series of all voxels within contrast-enhancing tumor mask. This average time series was then correlated with each voxel within tumor mask. Because mean time series of entire contrast-enhancing ROI is not identical to each contrast-enhancing voxel time series, correlation between two is less than 1.) **B,** Graph shows control time series has highest correlation with control regions and no correlation with tumor. All pairwise comparisons are significant.

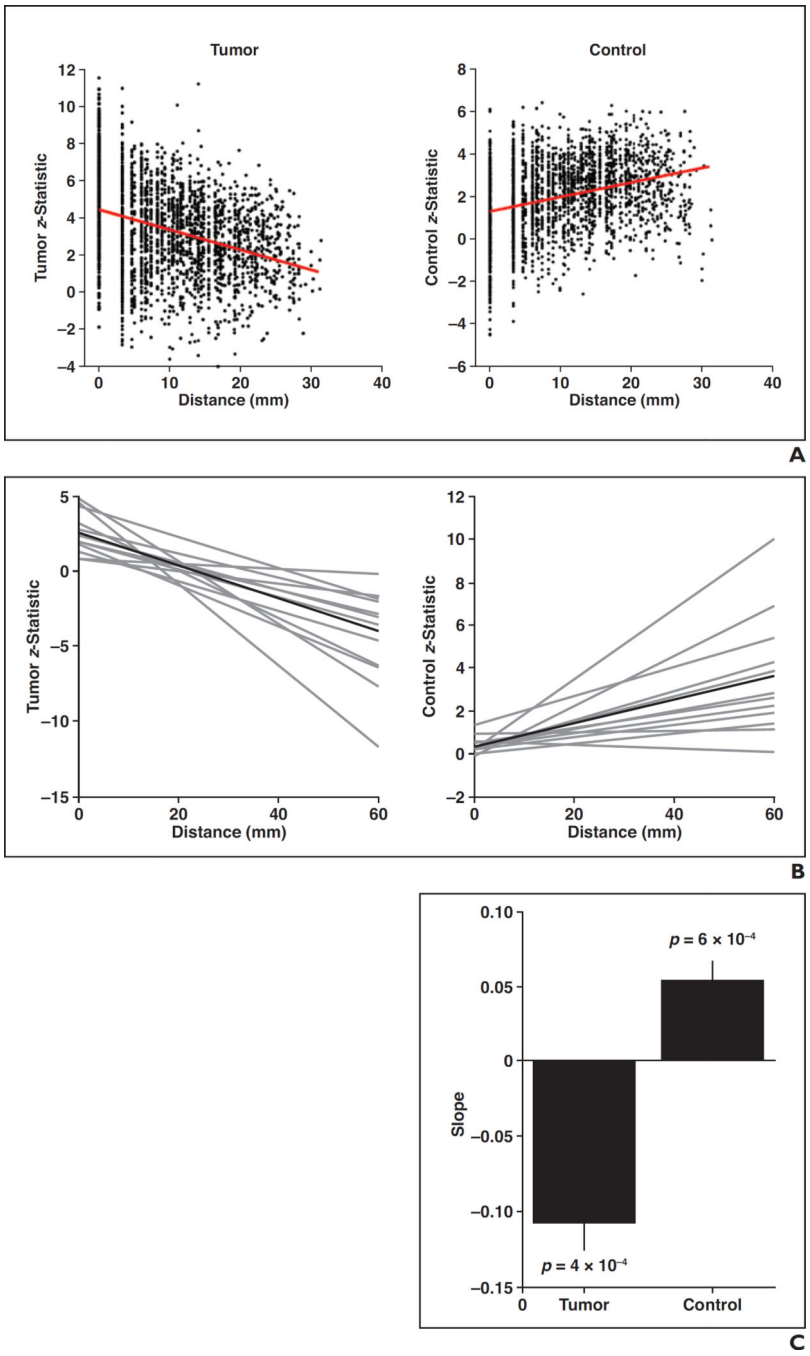

Fig. 4. Effect of distance

A, Scatterplots show *z*-statistics for all voxels in peritumoral region plotted as function of distance from nearest contrast-enhancing voxel for single patient. Tumor signal intensity has negative slope with distance, suggesting decreasing tumor gradient. Control signal intensity has opposite relation.

B, Graphs show slope lines for each patient (*gray*) and mean slope (*black*). All patients have negative tumor slope. All but one have positive control slope.

C, Graph shows both negative tumor slope and positive control slope are significantly different from zero.

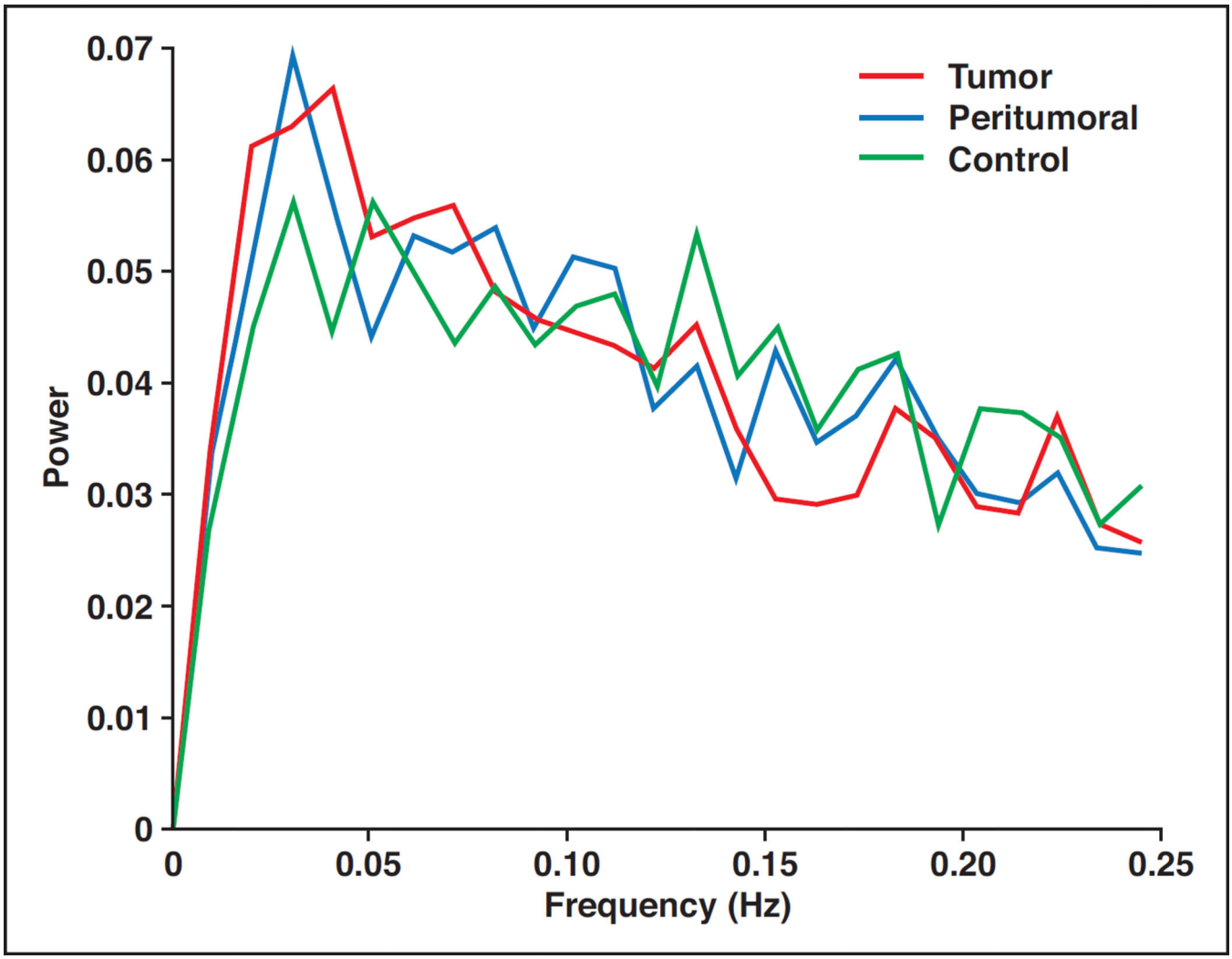

Fig. 5. Graph shows spectral dynamics

When averaged across tumor and peritumoral masks, no significant differences in power were detected, suggesting that blood oxygenation level–dependent mechanism is intact and only correlations between regions are affected by tumor.

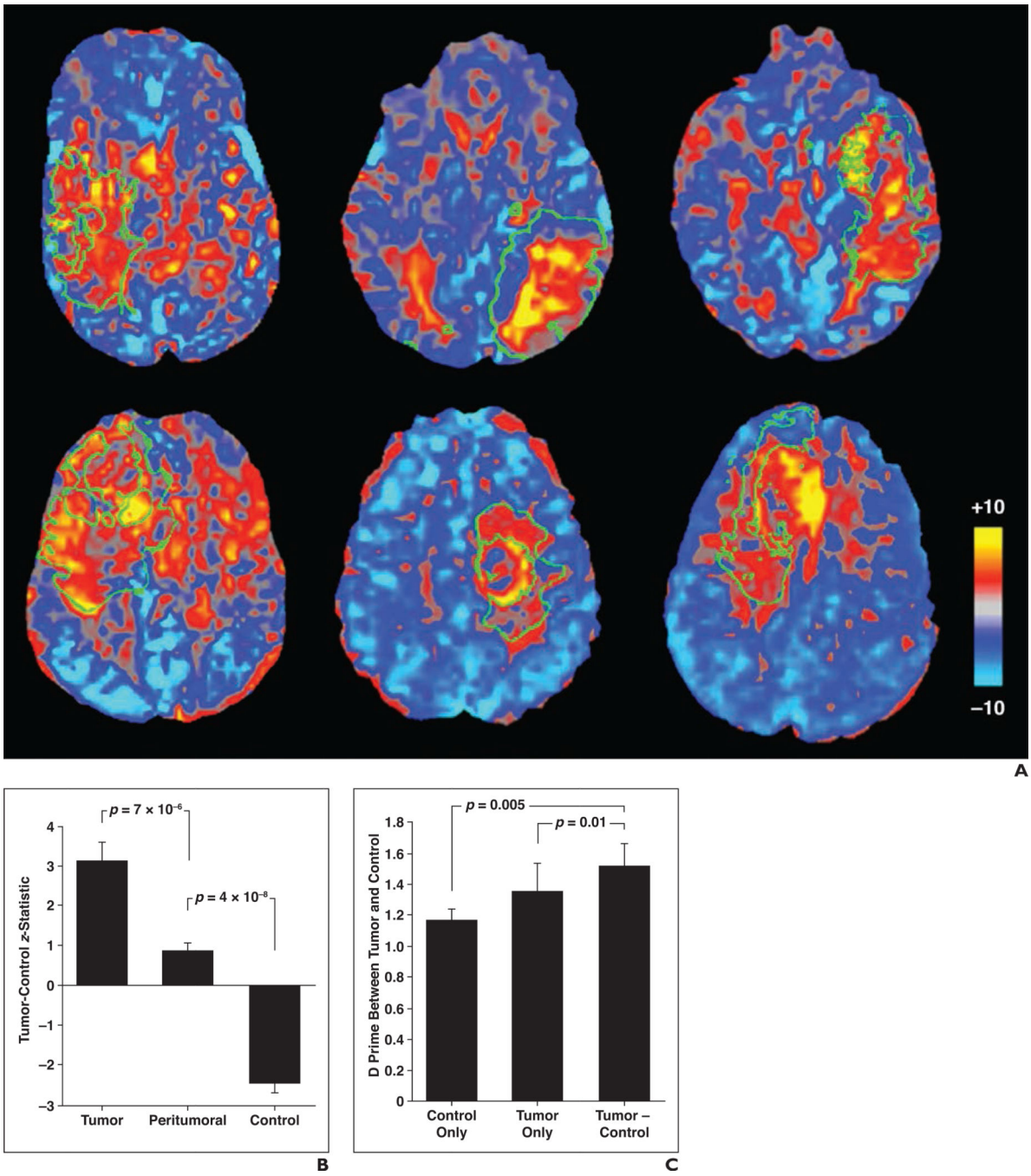

Fig. 6. Difference of tumor and control maps

A, *Left to right, top to bottom,* 44-year-old man, 35-year-old woman, 54-year-old man, 56-year-old man, 35-year-old man, 61-year-old man with glioblastoma. MR images show combining two statistics into one measure produces stronger separation between tissue types. Blue represents regions unaffected by tumor, and red appears to be localized to tumor and peritumoral region.

B, Graph shows group means exhibit significant differences in pairwise comparisons.

C, Graph shows image contrast between tumor and control regions significantly improves with combination of tumor-only and control-only images.